JOURNAL OF GEOPHYSICAL RESEARCH, VOL. 112, A06224, doi:10.1029/2006JA011918, 2007

Click Here for Full Article

Prediction of the *AL* index using solar wind parameters

Xinlin Li,[1,2,5] Kap Soo Oh,[1,3] and M. Temerin[4]

Received 14 June 2006; revised 28 January 2007; accepted 12 February 2007; published 15 June 2007.

[1] Two empirical models, one simple, one more complex, are introduced to predict the *AL* index, a measure of the Earth's auroral activity derived from magnetometers in the Northern hemisphere. Both models are based on solar wind and magnetometer data from the year 1995. The simple model predicts the 10-min averaged *AL* index for 1995 using only solar wind measurements with a prediction efficiency of 0.644 and a linear correlation of 0.803. The more complex model has a prediction efficiency of 0.723 and a linear correlation of 0.850. The simple model forward integrates with a 10-min time step the model *AL* term using a driver term on the basis of the solar wind magnetic field magnitude and direction, solar wind velocity and density, and a nonlinear decay term whose amplitude depends on the model *AL* amplitude. The more complex model adds annual, semiannual, and diurnal variations, saturation, and some time delays and an additional term that is a direct function of the solar wind magnetic field and velocity. Though both models were optimized to predict the 10-min averaged *AL* index, both models predict a longer-averaged *AL* index substantially better (prediction efficiency of 0.736 and 0.825, respectively, for the 2-hour averaged *AL* using the simple and complex models) while predicting the difference between 2-hour averaged *AL* and the 10-min *AL* poorly (prediction efficiency of 0.083 and 0.136, respectively) implying much less predictability for shorter timescale variations. The models show that the *AL* index is strongly dependent on the solar wind magnetic field and velocity but is practically independent of the solar wind density.

Citation: Li, X., K. S. Oh, and M. Temerin (2007), Prediction of the *AL* index using solar wind parameters, *J. Geophys. Res.*, *112*, A06224, doi:10.1029/2006JA011918.

1. Introduction

[2] Indices of large-scale magnetospheric activity, such as the hourly *Dst* index [e.g., *Burton et al.*, 1975; *Klimas et al.*, 1998; *O'Brien and McPherron*, 2000; *Temerin and Li*, 2002, 2006] or the radiation belt electron flux at geosynchronous orbit [e.g., *Baker et al.*, 1990; *Li et al.*, 2001a; *Li*, 2004], are quite predictable given solar wind conditions, and we have been making such predictions in real time for several years (e.g., http://lasp.colorado.edu/~lix/).

[3] Here we show our efforts to predict the *AL* index by making two models (simple and complex) of the 10-min averaged *AL* index using the solar wind as the only input for an almost continuous period of a year.

[1]Laboratory for Atmospheric and Space Physics, University of Colorado, Boulder, Colorado, USA.
[2]Department of Aerospace Engineering Sciences, University of Colorado, Boulder, Colorado, USA.
[3]Department of Astronomy and Space Science, Chungnam National University, Daejeon, South Korea.
[4]Berkeley, California, USA.
[5]Also at Laboratory for Space Weather, Chinese Academy of Sciences, Beijing, China.

Copyright 2007 by the American Geophysical Union.
0148-0227/07/2006JA011918$09.00

1.1. Auroral Indices

[4] The auroral electrojet indices have been widely used for monitoring geomagnetic activity and space weather and for research in geomagnetism, aeronomy, and solar-terrestrial physics since *Davis and Sugiura* [1966] introduced them to space physics. Since 1975, the auroral indices have been based on 1-min values of the northward H component magnetometer trace from 12 auroral observatories located between about 60 and 72 magnetic latitudes with a magnetic longitudinal spacing of 15°–50°.

[5] The auroral electrojet indices *AL*, *AU*, *AE*, and *AO* were introduced as a measure of the global auroral electrojet activity. The *AU* and *AL* indices were intended to express the strongest current intensity of the eastward and westward auroral electrojets, respectively. The *AE* index represents the overall activity of the electrojets, and the *AO* index provides a measure of the equivalent zonal current. The derivation of these indices is described in the World Data Center (WDC)-C2 Kyoto Web site.

1.2. Uncertainties in Auroral Electrojet Indices

[6] There are several deficiencies in the auroral electrojet indices that prevent the indices from being ideal measures of the auroral electrojet. The main deficiencies stem from longitudinal gaps in the distribution of the 12 observatories, from the small latitudinal range covered by each observatory,

from the offset of the local magnetic H component of an observatory with respect to the Earth's dipole north-south direction, and from the effects of strong local field-aligned currents in the substorm current wedge [*Clauer and McPherron*, 1974; *Baumjohann and Treumann*, 1999].

[7] At some magnetic observatories, the angle between the local magnetic H component and the global eccentric dipole north-south direction is greater than 30°. Since the electrojets tend to flow along the auroral oval, i.e., perpendicular to the global eccentric dipole north-south direction rather than perpendicular to the local H direction, these observatories tend to underestimate the electrojet current.

[8] The most severe longitudinal gap is in Siberia, spanning over 4 hours of local time, but there are also gaps in western Canada and in the Atlantic sector of more than 2 hours of local time. Substorm current wedges associated with weak or moderate substorms may cover less than 2 hours of local time and can be easily missed by the 12-station *AE* network [*McPherron et al.*, 1973; *Baker et al.*, 1996].

[9] Probably more severe is the small latitudinal range covered by the *AE* observatories. During times of weak activity, i.e., when the interplanetary magnetic field, IMF, is northward, the auroral oval contracts northward, and the electrojets flow poleward of 70° latitude. In this situation, the *AE* network, with all its stations south of 70°, may not detect any disturbance. Also, during major magnetic substorms, the auroral oval can expand equatorward below 60°, and the *AE* network will underestimate the strength of such events as well.

[10] As discussed above, the *AL* index is not a perfect index. Nonetheless, the *AL* index has been widely used in the community as a proxy for the auroral activity, and there has been a lot of effort to understand its variability and predictability.

1.3. Variations of Auroral Electrojet Indices

[11] The electrojet indices are known to have universal time [*Davis and Sugiura*, 1966; *Ahn et al.*, 2000a] and seasonal variations [*Russell and McPherron*, 1973; *Ahn et al.*, 2000b; *Lyatsky et al.*, 2001].

[12] The causes of the seasonal variation of geomagnetic activity has been reviewed by *Cliver et al.* [2000] and further investigated by *Li et al.* [2001b] and *Temerin and Li* [2002; 2006], where three causes are discussed: (1) the axial effect, that is the variation of the position of the Earth in heliographic latitude and the concurrent increase in solar wind speed at higher heliographic latitudes, (2) the equinoctial effect, that is the varying angle of the Earth's magnetic dipole axis with respect to the solar wind velocity and thus presumably a varying efficiency of coupling with the solar wind, and (3) the Russell-McPherron effect [*Russell and McPherron*, 1973], an effect due to the larger z component of the IMF near the equinoxes in geocentric solar magnetospheric (GSM) coordinates, which in turn is due to the tilt of the magnetic dipole axis with respect to the heliographic equatorial plane.

[13] Measurements of electric fields and Hall conductances such as done by the Chatanika radar [*Ahn et al.*, 1999] indicate that there are two sources of ionospheric conductance, one associated with the solar extreme ultraviolet (EUV) radiation, varying smoothly and maximizing near local noon, and the other associated with auroral particle precipitation, which shows a maximum around local midnight. The main contribution to the *AL* index is provided by *AE* stations in the post midnight-early morning sector [*Allen and Kroehl*, 1975], because of the contributions from both the substorm current wedge, which peaks near midnight, and the directly driven westward electrojet, which peaks around dawn. During expansion phase activity, the contribution to the *AL* jumps around between dawn and midnight depending on which component dominates. The average results put the peak in the *AL* index around 0300 Magnetic Local Time (MLT) as seen in the results of *Allen and Kroehl* [1975].

[14] *AU* and *AL* provide a measure of the maximum eastward and westward electrojet currents, respectively. *AU* and *AL* have different dependences on universal time and season. *AU* reflects the directly driven component of auroral activity, while *AL* contains significant contributions from both directly driven and substorm expansion phase activity. For these reasons, *Ahn et al.* [1999] and *Kamide and Rostoker* [2004] suggested that *AU* and *AL* be used as separate time series in all scientific studies. So here we focus on modeling the *AL* index instead of the *AE* index.

1.4. Previous Work on Predicting Auroral Indices

[15] The auroral electrojet indices have been predicted and reviewed by many people [e.g., *Baker*, 1986; *Clauer*, 1986]. We can divide the previous prediction models into two categories; (1) analogue models and (2) input-output data analysis models.

[16] A dynamical system can be expressed as a set of differential equations with several physical variables in analogue models, so the system can be understood physically. However, in input-output data-analysis models, the input to a physical system and its output response are used to determined the coupling characteristics of the system. Thus this coupling function may not have a clear physical meaning.

1.4.1. Analogue Models

[17] *Goertz et al.* [1993] constructed the first nonlinear analogue of the coupling of solar wind to the electrojet. Their model consisted of two independent components: (1) the response of the eastward electrojet, as measured by the *AU* index, to the reconnection electric field at the frontside magnetopause and (2) the response of the westward electrojet, as measured by the *AL* index, to the electric field in the plasma sheet. Magnetosphere-ionosphere coupling occurred through Alfvén waves driven by changes in the magnetospheric electric field. They achieved an *AE* correlation coefficient of 0.92 for 10-min resolution data during a 48-hour period in May 1979 and a slightly lower correlation for *AL*. *McPherron and Rostoker* [1993], commenting on this result, concluded that the remarkably high correlation was the consequence of several factors special to this 2-day interval. Thus McPherron and Rostoker predicted that the model would not do as well for other intervals.

[18] The Faraday loop model [*Klimas et al.*, 1992, 1994] is a time-dependent representation of magnetotail convection with a superposed loading-unloading cycle. A Faraday loop, which encircles one of the tail lobes, is used to relate changes in the magnetic flux in the lobe to electric potentials around the loop by Faraday's law, which are then expressed in terms of solar wind parameters and cross-tail currents. To relate the model output of the electric field to

the measured electrojet index data, an elementary mapping [*Weimer*, 1994] of the cross-tail electric field to the westward electrojet strength (*AL*) was added to the model. *Klimas et al.* [1994] found a correlation coefficient of about 0.65 for three consecutive intervals of the *Bargatze et al.* [1985] data set with a total of 140 hours of data. The Bargatze data set has a time resolution of 2.5 min.

1.4.2. Input-Output Data Analysis Models

[19] The linear prediction filter (LPF) technique was adapted by *Bargatze et al.* [1985] to analyze *AL* data. They assumed a linear relationship between an input time series and an output time series. The output was the *AL* index while the input was VB_s where V is the solar wind speed and B_s is the z component of the IMF when it is directed southward or zero otherwise. These data were used to find the best LPF for the data of November 1973 to December 1974. However, their results also showed that the relationship between VB_s and *AL* is nonlinear and is, as such, beyond the scope of the LPF technique.

[20] The local-linear prediction technique is an extension of the linear prediction filter technique that allows for nonlinear coupling. In this technique, a linear approximation to the nonlinear curve is constructed and used to predict the next step in the evolution of the simple magnetosphere. In practice, both the present and past inputs to the magnetosphere and its present and past geomagnetic activity outputs are used as inputs to the method to predict the future activity output. *Vassiliadis et al.* [1995] applied this technique to three intervals, a total 40 hours, of the *Bargatze et al.* [1985] data set and got a correlation coefficient of about 0.79 for 2.5-min resolution data and 0.87 for 25-min resolution data.

[21] Considerable success has been realized recently in studies of neural network-based predictions of magnetospheric storm conditions. The emphasis in such work is on prediction rather than on magnetospheric dynamics. The input and output data are coupled by an active function which is locally and globally nonlinear. *Hernandez et al.* [1993] have used neural nets to construct nonlinear models to forecast the *AL* index using the VB_s and *AL* data from *Bargatze et al.* [1985] for the input and output to their models. Using the state space reconstruction approach, which is a generalization of autoregressive-moving average models, they obtained a correlation coefficient of 0.91 for 15-min resolution for one interval of 47 hours in the Bargatze et al. data set. For the same data, *Weigel et al.* [2003] adapted the gated neural network with inputs of previously measured data and got a correlation coefficient of 0.94 for 15-min resolution data for one interval.

[22] More recently, *Chen and Sharma* [2006] introduced a new technique for data-driven modeling on the basis of the distance of the nearest neighbors from the current states, in which the contributions of the nearest neighbors are weighted by factors inversely proportional to the distances. They conclude that this technique yields better predictions, especially during strongly driven events [*Chen and Sharma*, 2006].

1.5. Motivation

[23] *Temerin and Li* [2002, 2006] developed an empirical model to predict the hourly *Dst* index. For the 8 years, 1995–2002, they obtained a prediction efficiency of 0.914 and a linear correlation coefficient of 0.956. They showed that the magnetosphere is highly predictable and that chaotic behavior within the magnetosphere has little influence on the large-scale currents that determine *Dst*. These results lead to the question, which this paper attempts to answer, of how a similar technique applied to the smaller-scale currents and shorter-timescales related to the auroral electrojet would work.

[24] *Shen et al.* [2002] have developed a relationship between the *AL* and *Dst* indices on the basis of the physics of the processes involved in order to understand the storm-substorm relationship. They argue that the magnetospheric electric field causes both the westward auroral electrojet and the particle injection into the ring current region. With the assumption that the magnetospheric electric field is homogeneous from the initial injection region through the ring current region, they produced a model of *Dst* on the basis of *AL* and the solar wind dynamic pressure. They found that the correlation coefficients between modeled *Dst* and the *Dst* index are 0.84 and 0.80 for 1998 and 1999, respectively.

[25] Figure 1 shows an example of the correlation between *Dst* and *AL* for days 80–120 of 1995. The figure shows that both indices respond in some ways similarly but that *AL* has much more variability. For all of 1995, the linear correlation coefficient between *Dst* and the 1-hour averaged *AL* is 0.62.

[26] These correlations between the *AL* and *Dst* indices motivated us to pursue the possibility that a modification of Temerin and Li's empirical method of predicting *Dst* could also predict the *AL* index well.

2. Model and Parameters

2.1. Data

[27] Almost continuous solar wind data are available from the Wind spacecraft since end of 1994 and through all of 1995. The perigee of Wind is sometimes inside the magnetosphere, so the 7% of data from 1995 could not be used. In our model, all solar wind data have been rotated into the GSM coordinate system, and the time of the solar wind has been changed to $t = t_{sw} - x/v_x$ (x, x component of solar wind location at t_{sw}; v_x, the magnitude of x component of the solar wind velocity at t_{sw}) to take into account the propagation of the solar wind to the Earth.

[28] In our calculations, we have used solar wind data interpolated to a constant 10-min interval (this is the same solar wind data set we used for the *Dst* prediction). We used the *AL* index data from the WDC (Geomagnetism, Kyoto). The last provisional *AL* index data currently available at the WDC are for 1995, so we modeled the 1995 provisional *AL* index after averaging the *AL* data to a 10-min interval.

[29] We developed two models of *AL* using the solar wind as input: a simple model which we call the "Simple Model" and a more complicated model which we call the "Complex Model". The Simple Model illustrates the basic connection of the solar wind parameters to the *AL* index. The Complex Model was made in order to include and investigate additional effects: annual, semiannual, and diurnal modulations, saturation, and some effects based on the past history of the solar wind and includes optimal smoothing. The simple model gives a root mean square (RMS) error between the prediction and the 10-min *AL* index of 99.6 nT, a prediction efficiency of 0.644, and linear correlation

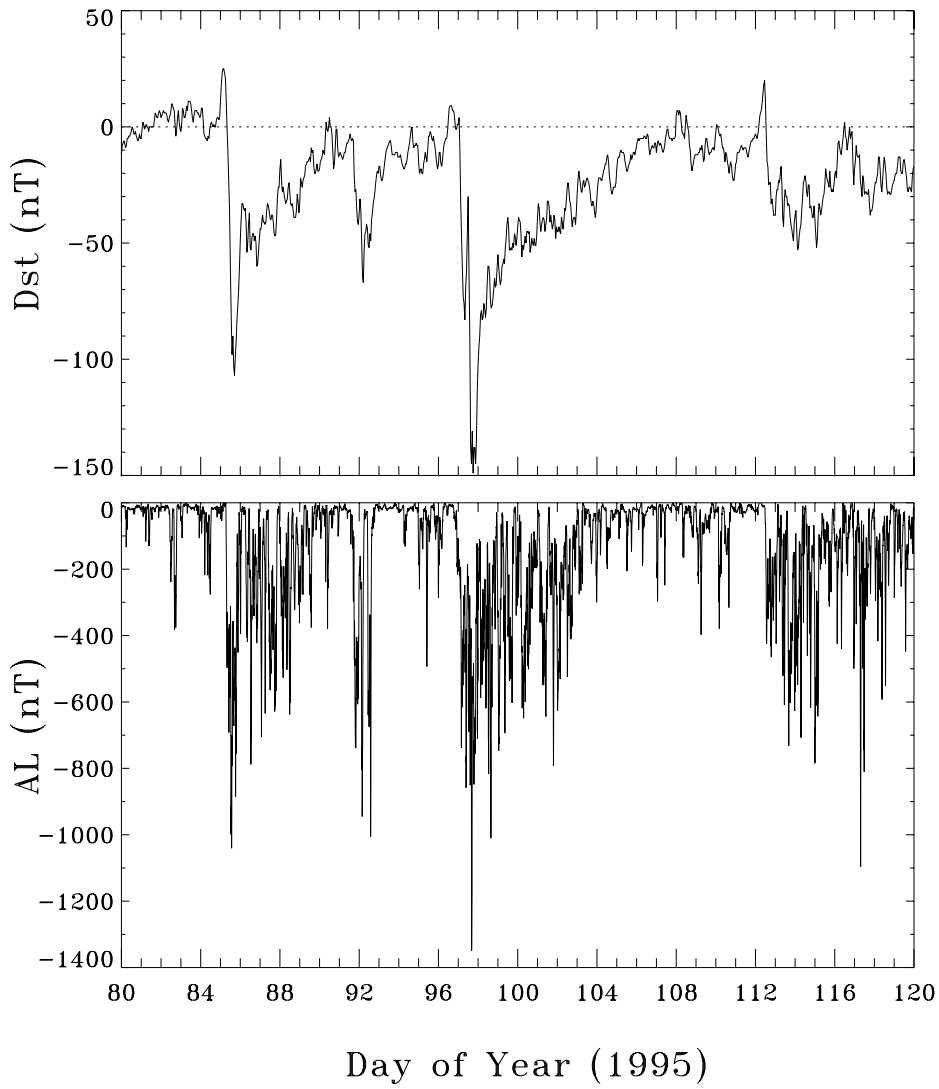

Figure 1. Comparison between Dst (an hourly index) and the10-min averaged *AL* index for days 80–120 of 1995.

coefficient of 0.803. The respective numbers for the complex model are 87.9 nT, 0.723, and 0.850. Thus about a quarter of the error that remains in the simple model, as measured by the prediction efficiency or correlation coefficient, is eliminated in the more complex model.

2.2. Simple Model

[30] The simple model of the *AL* index is calculated as:

$$AL_s(t) = \mathrm{al1}(t) + 24.94\mathrm{nT}, \quad (1)$$

where al1 is found by forward integrating al1 on the basis of solar wind data, 24.94 nT is a constant offset, and AL_s is the output of the simple model. The addition of a positive constant allows for AL_s occasionally to be positive. Since the *AL* index is usually negative, positive AL_s values are set to zero.

[31] The quantity al1 is found every 10 min for all of 1995 as follows:

$$\mathrm{al1}(t + \mathrm{dt}) = \mathrm{al1}(t) + (\mathrm{df1}(t) + 2.101*(\mathrm{abs}(\mathrm{al1}(t)))^{1.41})\mathrm{dt}, \quad (2)$$

where dt is 10 min or since time here is in days, dt = 0.0069444, and al1 is initialized with a value of −8 nT, though the exact initial value makes little difference. The last term in equation (2) produces a nonlinear decay whose timescale depends on the amplitude of al1. For al1 = −100 nT, the decay timescale is 1.73 hours; for a al1 = −500nT, the decay timescale is 0.89 hours.

[32] The term df1(t) is given as follows:

$$\mathrm{df1}(t) = -2474.5*\mathrm{bt}^{0.90}*(\sin\theta)^{4.85}*(v_x/430.0)^{2.14}*(n/7.0)^{0.05}, \quad (3)$$

where n is solar wind density in ions/cm^3, v_x is the solar wind velocity along Sun-Earth line in km/s, and bt is the magnitude of the IMF in nanoTesla in the plane perpendicular to the Sun-Earth line and $\theta = -(\mathrm{acos}(-\mathrm{bz}/\mathrm{bt}) - \pi)/2$ where bz is the z component of the IMF in GSM coordinates.

[33] An example of the model output is shown in Figure 2. In comparing the model with the measured *AL* index, there

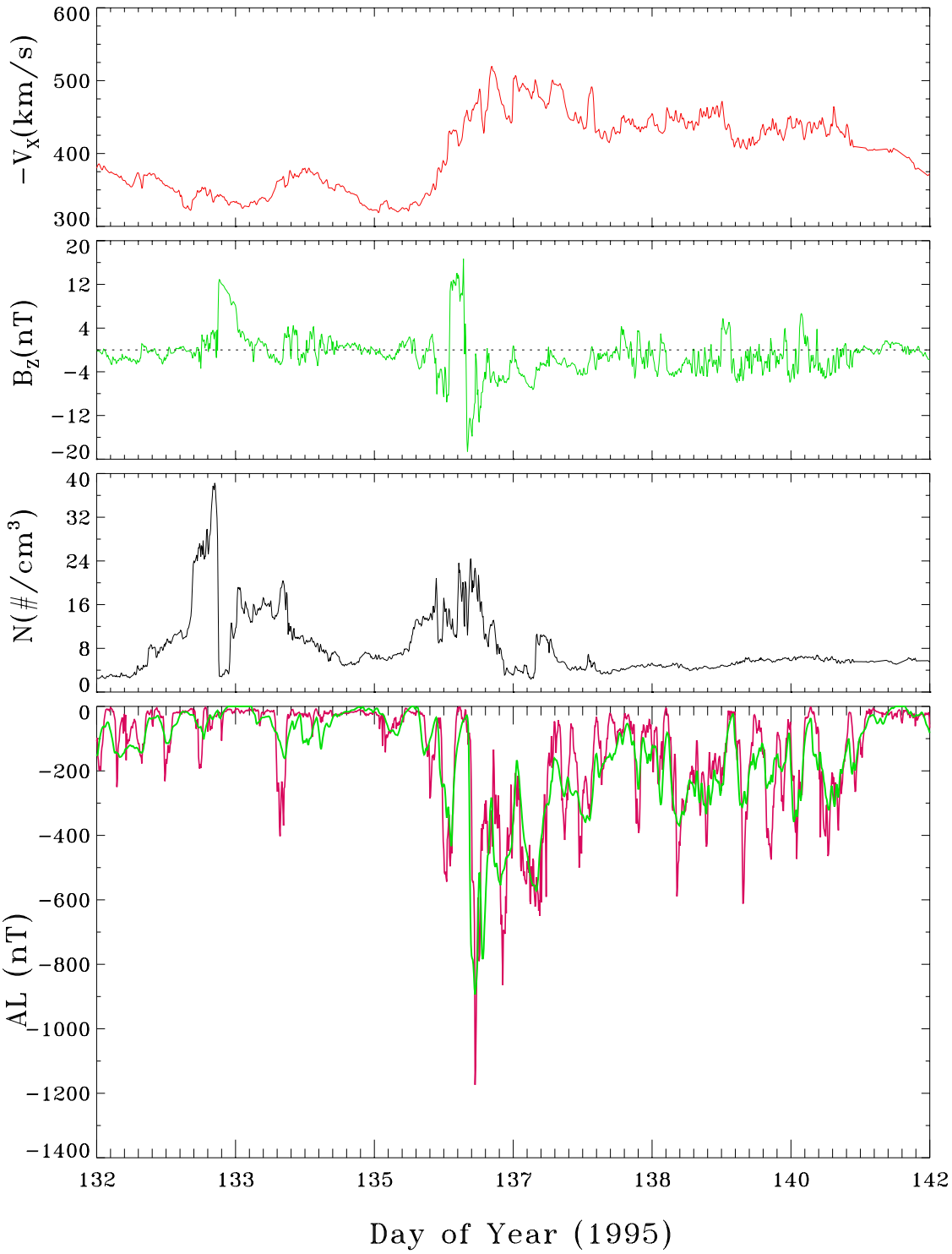

Figure 2. Relevant solar wind parameters and a comparison between the measured *AL* index (10-min averaged, red) and the predicted *AL* index (green) from the simple model for days 132–142 of 1995.

is an additional parameter that is optimized which is the time shift between the model output and the *AL* index. For the simple model, there is delay of 7.30 min added to the model output (that is, the nominal model output at 10 min is compared with the *AL* index at 17.3 min); for the more complex model, this time will be 7.42 min. The time delays are quoted at better than 10-min resolution because the model output is interpolated before comparison with the *AL* index.

[34] In equations (1), (2), and (3), all numerical values were found by minimizing the RMS error between the model prediction and the 10-min averaged *AL* index. The RMS error for all of 1995 (excluding intervals for which there was no solar wind data) was 99.56 nT, the prediction

efficiency (PE), defined as (PE = [1−(mean squared residual)/(variance of data)]) was 0.644, and the linear correlation between the model and the 10-min averaged *AL* index was 0.803.

[35] For typical solar wind values, $v_x = 430$ km/s, $n = 7/\mathrm{cm}^3$, bt = 5nT, and a southward IMF such that $(\sin\theta)^{4.85} = 1$, we find that a typical change for the *AL* index initially at zero during a 10-min time step is given by

$$\mathrm{df1{*}dt} = -2474.5{*}(5^{0.90}){*}6.9444{*}10^{-3}\mathrm{nT} \approx -73\mathrm{nT} \quad (4)$$

Equation (3) shows that AL_s, and thus by implication the *AL* index, is practically independent of the solar wind density-$(n/7.0)^{0.05}\sim 1.0$ for all typical values of solar wind density, and has strong dependence on v_x and a somewhat less strong dependence on bt. However, the variability of bt and of angular factor $\sin\theta$ are much greater than the variability of v_x, and thus the variability of the IMF dominates the variability of *AL* especially on shorter timescales.

[36] The simple model of *AL* provides the basic description of how auroral activity as measured by *AL* depends on solar wind parameters and helps one to see the relative significance of various solar wind parameters affecting the *AL* index. It is also expected that the *AL* index should have annual, semiannual, and diurnal variations and that there may be additional time delays in the response of the magnetosphere to the solar wind. To explore these issues and see how much more one can improve the model, we have included some of these factors into the more complicated model.

2.3. Complex Model

[37] The more complicated model is given by:

$$\begin{aligned} AL_c(t) =& (\mathrm{al}(t) + \mathrm{al2}(t))(1 + 0.112{*}\sin(2\pi t + 4.17) \\ & \cdot (1.0 + 1.72{*}\sin(t{*}\mathrm{fy} + 2.03))) \\ & \cdot (1 + 0.038{*}\sin(4\pi t + 1.09)) - 9.868\mathrm{nT}, \end{aligned} \quad (5)$$

where fy = $2\pi/365.24$.

[38] This equation shows that the output of the more complicated model ($AL_c(t)$) is the sum of two terms (al and al2) whose amplitude is modulated by a diurnal and semidiurnal term. The term al is basically determined by forward integration, while the term al2 is directly calculated from the solar wind v_x and bz values. The first "sine" term gives a nominal diurnal variation to AL_c of 11% such that AL_c is typically largest at 14 UT or when Canada is in the morning sector. However, the second "sine" term gives an annual modulation to the amplitude of the diurnal variation, such that the diurnal variation actually varies and is largest around 5 December with an amplitude of 30.5% (0.112*2.72) and reverses sign and has an amplitude of 8.1% around 5 June. Thus near the winter solstice, there is a larger diurnal variation than near the summer solstice. The last "sine" term provides for a semidiurnal variation, and the amplitude of the term shows that the semidiurnal variation is small.

[39] We describe the calculation of the al2(t) term, which is the smaller of the two terms, in several steps. First we calculate al2′, then al2″, etc.

$$\begin{aligned} \mathrm{al2}'(t) =& (\sin\phi{*}(t - 0.0625))^{2.76}{*}(-12.21{*}\mathrm{bz}(t - 0.0625) \\ & {*}(v_x(t - 0.0625)/430.0)^{1.55}{*} + 19.44{*}\mathrm{bz}(t - 0.0556) \\ & {*}(v_x(t - 0.0556)/430.0)^{1.55}) \end{aligned} \quad (6)$$

Equation (6) says that al2′ (and thus al2) depends on the solar wind bz and v_x values 80 min (i. e., at time $(t - 0.0556)$) and 90 min (i. e., at time $(t - 0.0625)$) before and on $\sin\phi$ where $\sin\phi = \sqrt{(1 - \cos\phi^2)}$ and

$$\begin{aligned} \cos\phi =& \sin(t{*}\mathrm{fy} + 0.2026){*}0.0366{*}\sin(2\pi t - t{*}\mathrm{fy} - 1.603) \\ & + \cos(t{*}\mathrm{fy} + 0.2026) \\ & {*}(0.39 + 0.040{*}\cos(2\pi t - t{*}\mathrm{fy} - 1.603)) \end{aligned} \quad (7)$$

The term $\sin\phi$ is nominally the sine of the angle between the magnetic dipole axis and the Sun-Earth line, depends on the rotation phase of the Earth because of the offset of the dipole axis from the rotation axis, and depends on the revolution phase of Earth around the Sun because of the tilt of the rotation axis with respect to the ecliptic plane. However, in our fitting procedure, the revolution angle (here 0.2026 radians), the rotation angle (here −1.603 radians), and the magnitude of the offset of the dipole axis from the rotation axis (here reflected by the value 0.0366 and 0.040 corresponding to an offset of 2.29°) were free parameters. The rotation and revolution angles correspond to a $\sin\phi$ minimum at 6 UT on 20 December and another minimum 6 months and 12 hours later. This term gives the equinoctial effect [*Cliver et al.*, 2000; *Li et al.*, 2001b] and gives a maximum in auroral activity near the equinoxes and minimum at the solstices. There is a corresponding term of larger amplitude that affects the driver term of al. The modulation due to that term, $(\sin\phi(t))^{6.30}$ used in equation (14), is illustrated in Figure 3. Since al is by far the dominant term, its modulation by $(\sin\phi(t))^{6.30}$ approximates the overall modulation of the model *AL* because of the equinoctial effect. Because the magnetic dipole axis is offset from the rotation axis by only 2.29° instead of the actual 11°, the diurnal modulation is much less than expected from the equinoctial effect. However, one must consider that there is an additional diurnal variation due to equation (5).

[40] From al2′, we then calculate al2″ as follows:

$$\mathrm{al2}''(t) = \mathrm{al2}'(t)(1.0 + 1.10{*}\sin(t{*}\mathrm{fy} + 5.13)), \quad (8)$$

[41] This provides for an annual variation that appears to be quite large (110%). However, there is also an annual variation in the al term of about 21.8% with almost an opposite yearly phase, and since the al term is substantially larger than the al2 term, the two annual modulations partly cancel. The overall annual modulation of AL_c is small, about 6%, with a maximum around 1 August. The effect of this annual modulation on al2 is such that the al2 term contributes little to the overall prediction in late fall and early winter but contributes substantially, though still less than the al term in late spring and early summer.

[42] From al2″ we then calculate al2″ as follows:

$$\mathrm{al2}'''(t) = \mathrm{al2}''(t) + 0.32 - \mathrm{abs}(\mathrm{al2}''(t) + 0.32) \quad (9)$$

This provides that if al2″ (and thus bz) is positive or only slightly negative (but not less than −0.32) that al2‴ will be zero. Thus the al2 term only has an effect for negative bz.

[43] Finally, al2 is calculated as

$$\mathrm{al2}(t) = \mathrm{smooth}^{21}(\mathrm{al2}'''(t), 3) \quad (10)$$

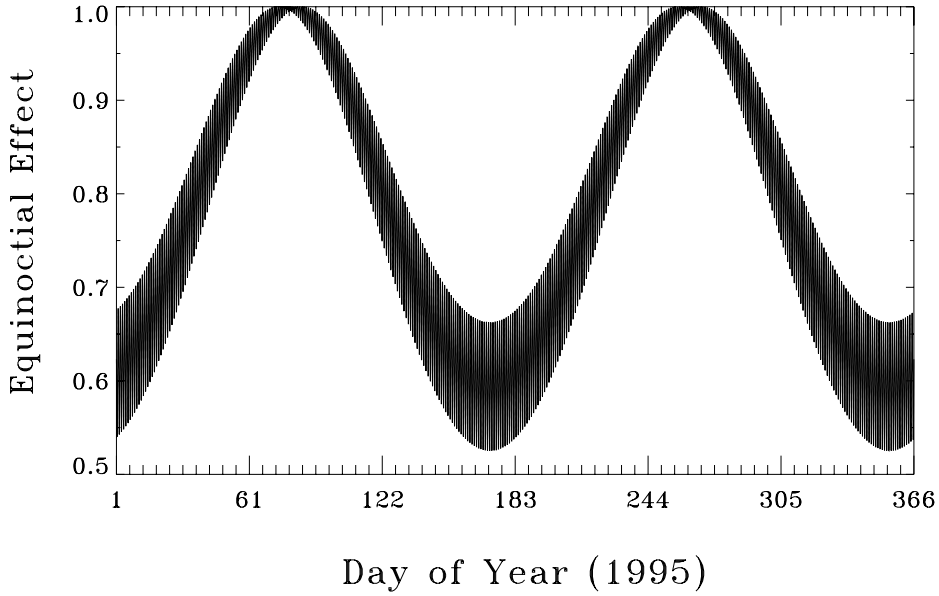

Figure 3. The semiannual and diurnal variation of the main driver term, which has a corresponding effect on the overall modulation of the model *AL* due to the equinoctial effect. The vertical thickness of the line represents the magnitude of the unresolved diurnal variation of the main driver term.

where smooth^{21}(al2$'''$ (t),3) means that the three-point smoothing function (i.e., three-point running average) is applied successively 21 times, essentially producing a Gaussian smoothing.

[44] The number of smoothings was determined by minimizing the RMS error of the prediction against the 10-min *AL* index. The smoothings imply, and we show more explicitly later, that the model cannot predict variations well on a short timescale.

[45] The term al is calculated as follows. First we calculate $a1$ as

$$\begin{aligned} a1(t+\mathrm{dt}) = & a1(t) + (10.688*(\mathrm{abs}(-a1(t)))^{1.196} \\ & *(1-0.00126*a1(t-0.0625)) + \mathrm{df2}(t) \\ & *(1-\mathrm{erf}(0.050*(\mathrm{bz}(t-0.0347)+0.29 \\ & *\mathrm{abs}(\mathrm{bz}(t-0.0347)))))*(1+0.00079*a1(t-0.0625)) \\ & *(1-0.00163*a1(t-0.0625)))*\mathrm{dt} \end{aligned} \tag{11}$$

and $a1$ is set to zero should it ever be greater than zero. Then $a2$ follows from $a1$ as

$$a2(t) = a1(t)*(1.0 + 0.218*\sin(t\mathrm{fy} + 2.19)) \tag{12}$$

and al follows from $a2$ as

$$\mathrm{al}(t) = \mathrm{smooth}^3(a2(t), 3) \tag{13}$$

where equation (12) provides for the annual variation, and equation (13) provides for the smoothing as discussed already in relation to the al2 term.

[46] An example of al and the al2 terms, including their diurnal modulations and their sum (−9.868 nT) as indicated by equation (5), and the measured *AL* index are shown in Figure 4.

[47] Equation (11) implements the forward integration of the main contribution to AL_c. The first part of the second term on the right hand side of equation (11) provides for the nonlinear decay of $a1$. An additional factor in the decay term enhances the decay on the basis of the amplitude of $a1$ 90 min (0.0625 day) earlier. Ignoring this term, one can estimate the time constant of the decay of $a1$ (and thus AL_c since $a1$ is usually only slightly less than AL_c). For $a1$ = −100 nT and −500 nT, the decay timescale is 0.91 hours and 0.66 hours, respectively.

[48] The factor df2 is a function of the solar wind parameters and is approximately equal to the driver term. However, the value of the driver term is here modulated by the value of bz 50 min (0.0347 day) earlier and by the value of $a1$ 90 min (0.0625 day) earlier. The modifications of equation (11) due to earlier values of $a1$ and bz only slightly improve the model results while greatly complicating the appearance of the equation. However, we keep the terms to demonstrate the kind of things we tried to do to improve the model.

[49] In equation (11), df2(t) is given by:

$$\mathrm{df2}(t) = 38076*(\sin\phi(t))^{6.30}*\mathrm{fe2}(t)/(1. - \mathrm{fe2}(t)) \tag{14}$$

where $(\sin\phi(t))^{6.30}$ provides for the equinoctial effect in the driver term of equation (11) as previously discussed and fe2(t)/(1. − fe2(t)) provides for saturation for larger negative values of fe2 (fe2 is always negative) such that df2 can never be less than −38076, and thus the magnitude of df2*dt in equation (11) cannot exceed 264.4 nT per a 10-min time step.

[50] The fe2 term is in turn given by:

$$\mathrm{fe2}(t) = \mathrm{fe1}(t) + (\mathrm{fe1}(t) - \mathrm{fe1}(t-0.0347))*0.077 \tag{15}$$

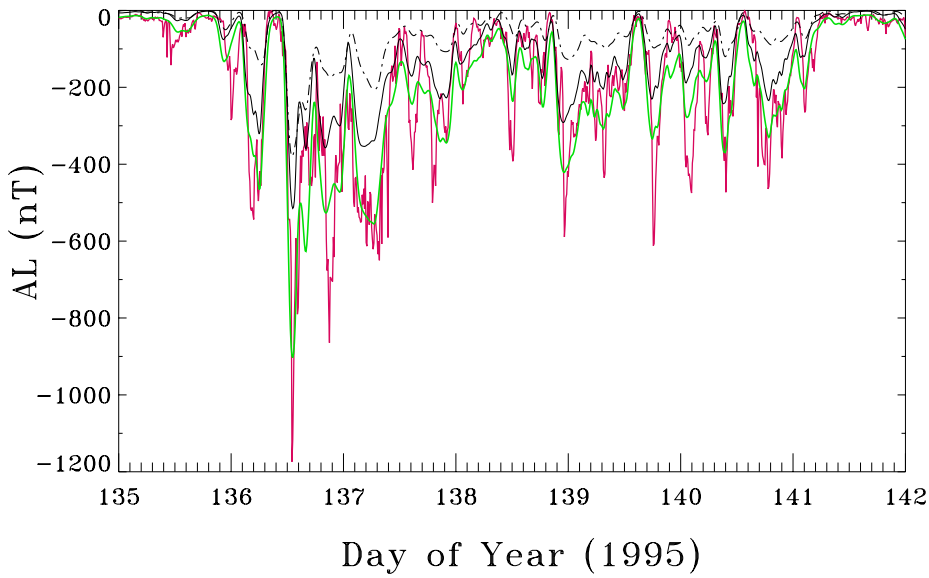

Figure 4. In the complex model, the *AL* is the sum of two terms, al and al2 (and −9.868 nT), as indicated by equation (5). An example of al (solid black), al2 (dash dotted black), the modeled *AL* (green), and the measured *AL* (red) for days 135–142 of 1995.

This equation provides that the magnitude of the fe2 term at time t is slightly larger than the magnitude of the fe1 term at time t, provided the magnitude fe1 is larger than its magnitude 50 min previously and vice versa.

[51] The term fe1 has the following dependence on the main solar wind parameters:

$$\begin{aligned}\mathrm{fe1} = &-5.529{*}10^{-2}{*}\mathrm{bt}(t)^{1.530}{*}(\sin\phi(t))^{6.51}{*}(v_x(t)/430.)^{4.10}\\ &{*}(n(t)/7.)^{0.170}{*}(1.+\mathrm{erf}(0.0444{*}\mathrm{dh}(t){*}\mathrm{bp}(t)\\ &{*}\cos(\mathrm{ang}(t)+0.03)))\end{aligned} \tag{16}$$

and, except for the last factor and that all the terms are raised to higher powers, is similar to equation (3). In the last term, bp is the magnitude of the IMF in the GSM x-y plane (i.e., bp = $\sqrt{(by^2+bx^2)}$) and ang = $a$tan(bx,by), and thus bp(t)*cos(ang(t)+0.03) is essentially by. The term dh is given by

$$\mathrm{dh}(t) = 1.43{*}\cos(t{*}\mathrm{fy}-0.061)+\sin(2\pi t+0.52) \tag{17}$$

and thus depends on the annual and diurnal phases.

[52] The higher power for all of the solar wind terms in the complex model versus the simple model is due to the addition of the saturation term [equation (14)] in the complex model. The saturation term allows the driver to become larger since then the saturation term is applied to reduce it. For an easier comparison with the simple model, one can rewrite equation (16) as:

$$\begin{aligned}\mathrm{fe1}(t) = &-5.529{*}10^{-2}{*}\{\mathrm{bt}(t)^{0.90}{*}(\sin\theta(t))^{3.83}{*}(v_x(t)/430.)^{2.41}\\ &{*}(n(t)/7.)^{0.1}\}^{1.7}{*}(1.+\mathrm{erf}(0.0444{*}\mathrm{dh}(t){*}\mathrm{bp}(t)\\ &{*}\cos(\mathrm{ang}(t)+0.03)))\end{aligned} \tag{18}$$

In equation (18), an overall power of 1.7 has been applied to the product of all the driver factors that were in the simple model, and the remaining powers are now much closer to those that were in the simple model.

[53] For a purely southward IMF and with the magnetic dipole perpendicular to the Sun-Earth line and with n = 7/cm^3 and v_x = 430 km/s and ignoring terms with past history of fe1 and bz, one can combine equation (11) with equations (16) and (14) to get a simpler expression for equation (11) in terms of bz.

$$\begin{aligned}a1(t+\mathrm{dt}) = &a1(t)+(10.688{*}(-a1(t))^{1.196}-2105{*}(-\mathrm{bz})^{1.53}\\ &/(1+.0553{*}(-\mathrm{bz})^{1.53}))*\mathrm{dt}.\end{aligned} \tag{19}$$

The term with bz is the driver term in the equation (if bz > 0, bz is set to be zero), and multiplying by dt to get the change in $a1$ due to this term in a 10-min interval, one gets

$$\begin{aligned}\Delta(a1) &= a1(t+\mathrm{dt})-a1(t)\\ &= -14.6{*}(-\mathrm{bz})^{1.53}/(1+.0553{*}(-\mathrm{bz})^{1.53})+\mathrm{decayterm}.\end{aligned} \tag{20}$$

In the limit of large magnitudes of negative bz and ignoring the decay term, $\Delta(a1)$ asymptotes to −14.6/0.0553 = −264nT. This is approximately the largest possible change in the model *AL* value in a 10-min interval. The actual *AL* index can change more rapidly. In general, both the simple and complex models tend to underestimate the rapid decreases and increases in *AL*. Thus the decay term is also somewhat less steep than in the actual *AL* [*Weimer*, 1994]. The effect is to smooth out rapid changes in *AL* associated with substorms.

[54] The model predicts faster decay with larger amplitude in agreement with *Weimer* [1994] but in seeming contradiction to *Rostoker et al.* [1991], who found an opposite dependence and decay times of less than 20 min for small-amplitude events. However, this may be reconciled. Because the model does not predict short timescale

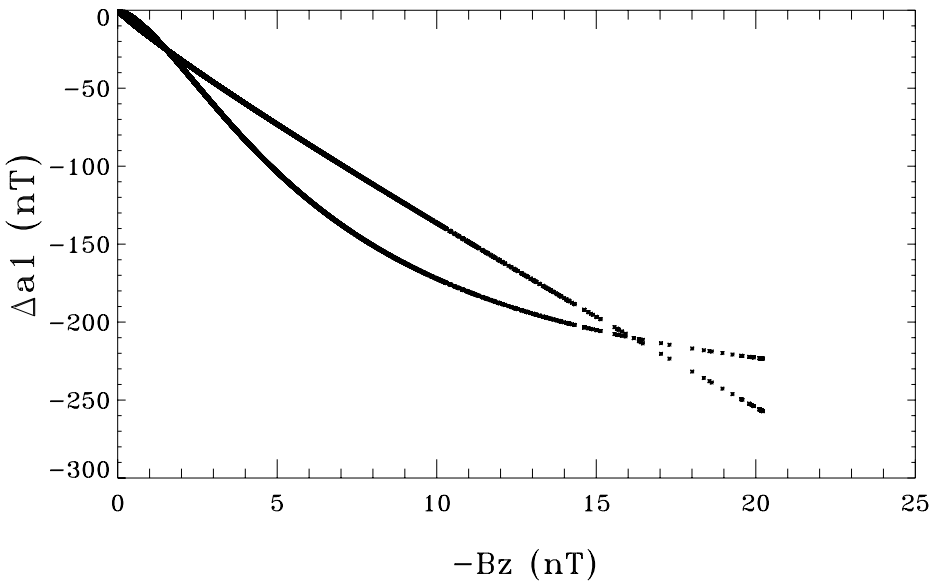

Figure 5. The magnitude of $\Delta(a1)$ (the curved line) and its equivalent for the simple model (the almost straight line) versus the magnitude of bz for negative bz, as indicated by equations (20) and (3), respectively, which show approximately how much *AL* changes as a function of negative bz in a 10-min interval for average solar wind parameters, $n = 7/\text{cm}^3$ and $v_x = 430$ km/s. Only values of bz that actually occurred in 1995 are used.

variations, the model cannot have decay times of the order of 20 min. This does not mean that short-scale variations are ignored. In the model, they are averaged over. Since the timing of enhancements in the magnitude of the *AL* index lasting a short time (of the order of 30 min) can only be predicted to within about 1.5 hours, they become 2-hour enhancements in the model but with smaller amplitudes so that, after averaging both the model and the data over 2 hours, everything more or less agrees. Another way to say this is that the model predicts the rise and fall of the expectation value of the *AL* index rather than the *AL* index itself, and so the model decay times do not necessarily correspond to the actual decay times of the *AL* index especially for short timescale events.

[55] Another feature of the complex model is saturation: very large solar wind inputs do not have correspondingly large effects on the *AL* index. Defining saturation in equation (20) as $1 + 0.00553 * (-\text{bz})^{1.53} = 2$, one gets that saturation occurs for bz = −6.63 nT, corresponding to a change in the model *AL* that is half the maximum. Saturation occurs for smaller values of bz if the velocity is larger than the assumed 430 km/s as it usually is for active magnetic intervals. For comparison, the average value of the magnitude of bz in the IMF near Earth is approximately 3 nT. Figure 5 shows the magnitude of $\Delta(a1)$ for a 10-min interval versus the magnitude of bz for negative bz [i.e., equation (20)], ignoring the decay term, and shows approximately how the modeled *AL* changes and how the change saturates as a function of negative bz in a 10-min interval, for the average solar wind parameters of $n = 7/\text{cm}^3$ and $v_x = 430$ km/s. In order to give an indication of the data used to derive this function, only bz values that were actually measured in 1995 are shown in Figure 5. Also shown is the corresponding function for the simple model, i.e., equation (3).

[56] Figure 6a shows another comparison of AL_c with the *AL* index. In general, AL_c falls more slowly and recovers more slowly than *AL* and underrepresents the peak excursion of *AL*. It would seem as if this would be an easy problem to correct by making the AL_c peak larger, but the problem is in the timing; the peak in such a larger, steeper AL_c would likely not coincide with the *AL* peak and thus would increase the RMS error of the model. We have not figured out how to make the peaks coincide more exactly. Since large negative excursions of *AL* are generally taken to represent substorms [e.g., *Weimer*, 1994], this means that while the model *AL* gives the overall integrated magnetic deflection during a substorm, the exact timing of the substorm is not predicted by our model.

3. Results and Discussions

[57] For 1995, both the solar wind data and the *AL* index (provisional version) are available. We have taken advantage of this coincidence to develop our models. These models not only show the effect of solar wind parameters on auroral activity as measured by the *AL* index but also show the magnitudes of the annual, semiannual, and diurnal modulations of the *AL* index and how the index saturates and how it decays. The model also shows those aspects of the *AL* index that are easily predictable and those aspects that are not so easily predictable using solar wind data.

[58] The model gives a smoother version of *AL*. In fact, the model has the best prediction efficiency when compared with the 13-point (2-hour, 10-min) running average of the *AL* index for which the model has a PE of 0.825, a RMS error of 61.1 nT, and a linear correlation coefficient of 0.910. The PE is even better when the 13-point running average of the model results is compared with the 13-point running average of the *AL* index: PE of 0.852, RMS error of

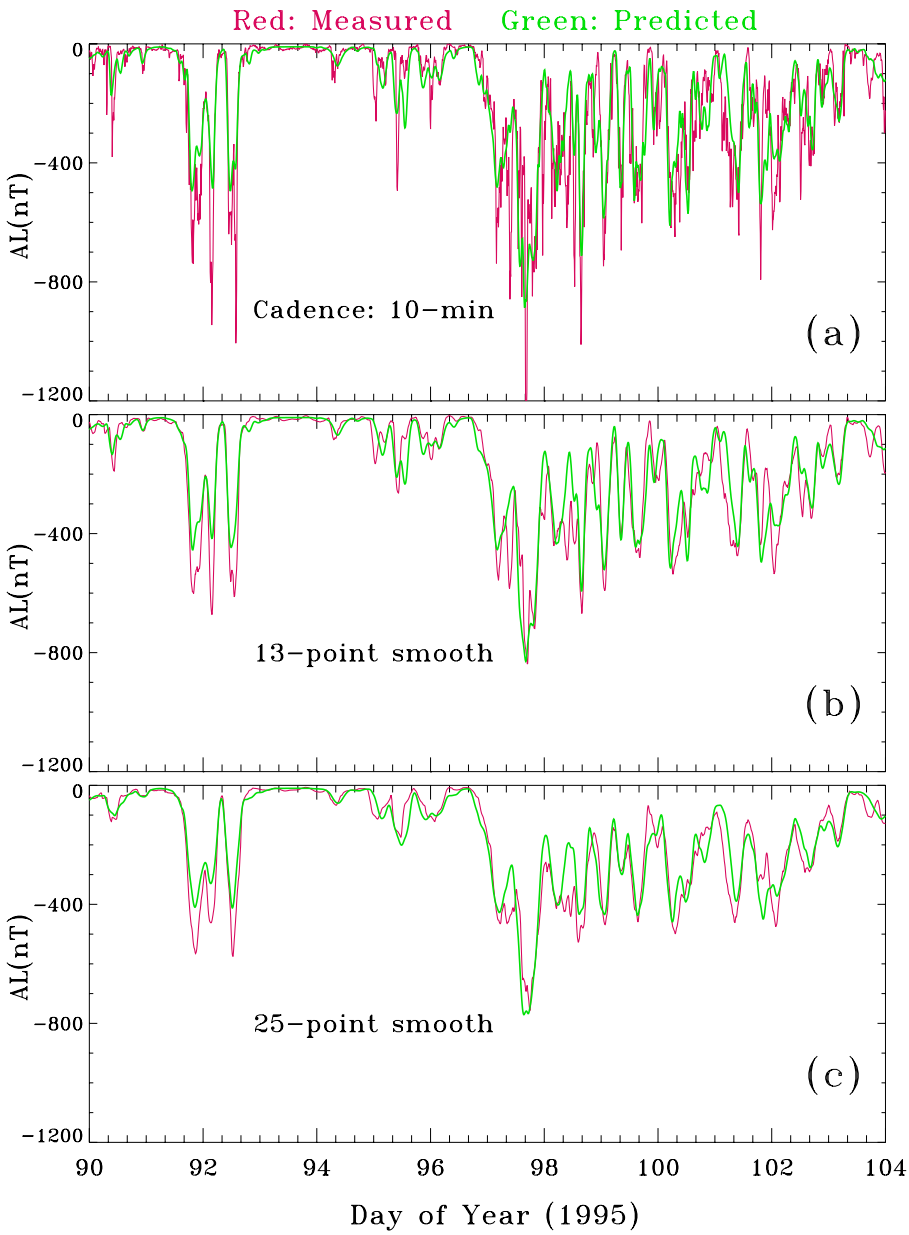

Figure 6. Comparison of the modeled *AL* from the complex model with the *AL* index. (a) Modeled *AL* (10-min resolution) and 10-min averaged *AL* index; (b) and (c) comparisons of the 13-point and 25-point running averages of the modeled *AL* and the 10-min averaged *AL* index.

56.1 nT, and a linear correlation coefficient of 0.923. The PE increases with greater averaging: for the 25-point running average of both the model and the *AL* index, the model gets a PE of 0.898, a RMS error of 42.7, and linear correlation coefficient of 0.947. Figures 6b and 6c illustrate the behavior of the model as the averaging is changed. Figure 7 provides a more complete view of the comparison between the 13-point running averages of the modeled *AL* and measured *AL* throughout 1995.

[59] In contrast, on short timescales, the model predicts poorly. The PE for the model minus its 13-point running average versus the *AL* index minus its 13-point running average is only 0.135, RMS error of 55.8 nT, and a linear correlation coefficient of 0.369. This is illustrated in Figure 8.

[60] A more exact way of looking at the timescale behavior of the *AL* index and of the model is to do a Fourier series analysis. Figure 9 shows the results of the 25-point running averaged power spectrum (which is basically the square of the so-called Fast Fourier Transform) of the *AL* index and of the model. The model has much less response at shorter timescales.

3.1. Sources of Error

[61] There are several sources of error. There is some uncertainty in the assumed propagation of the solar wind to the Earth [*Weimer et al.*, 2003; *Bargatze et al.*, 2005]. The *AL* index itself depends on the particular station that sees the largest current with respect to the auroral current system, and thus similar auroral currents can produce dissimilar

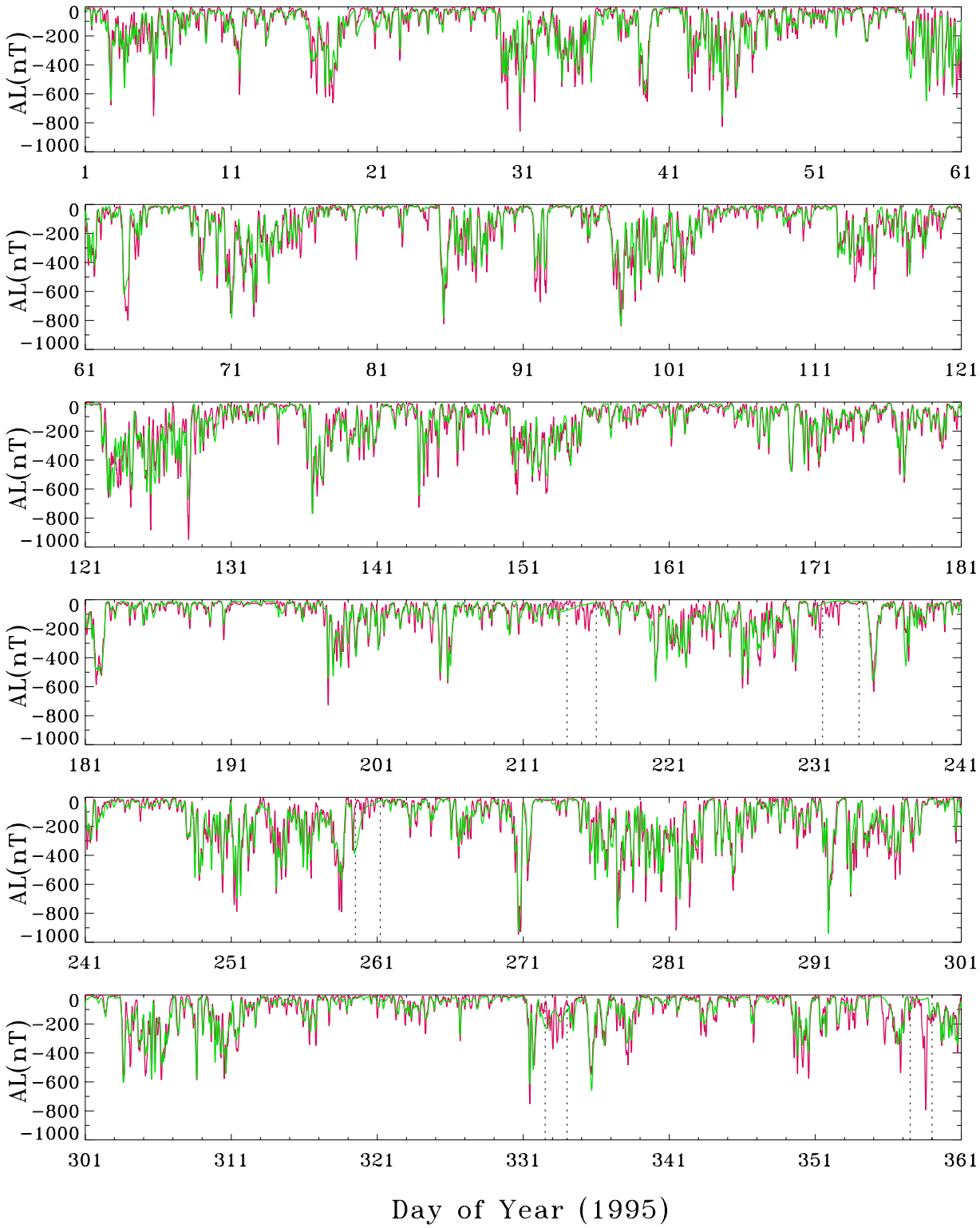

Figure 7. Comparison of the 13-point running average of the modeled *AL* (green) from the complex model with the 13-point running average of the *AL* index (red) for 1995.The Wind spacecraft came into the magnetosphere five times during 1995. These perigee passes (corresponding to solar wind data gaps) are indicated by the vertical dotted lines.

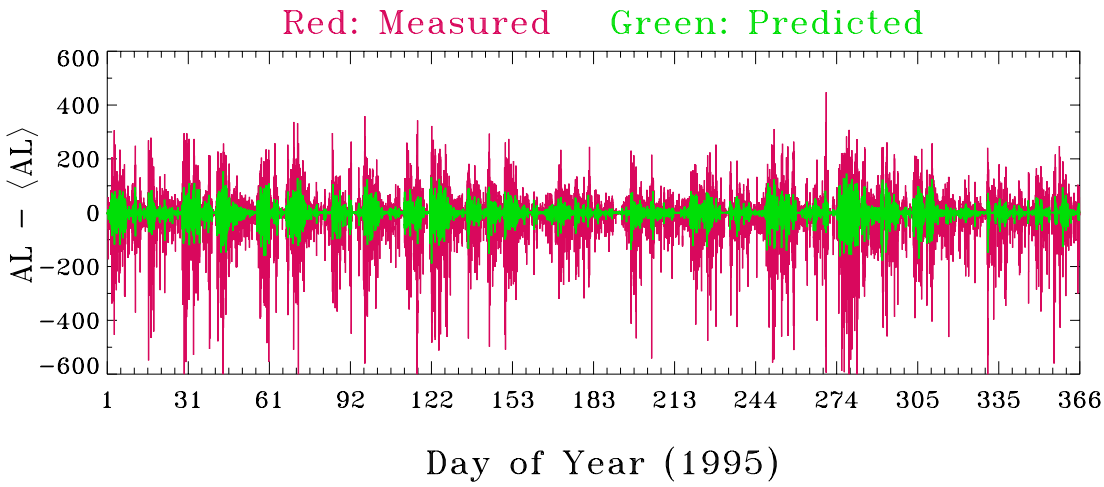

Figure 8. Comparison of the modeled *AL* minus its 13-point running average versus the *AL* index minus its 13-point running average for 1995.

values of *AL* depending on the relative location of that station.

[62] However, these are technical matters that could be corrected, in principal, with better auroral and solar wind data. More fundamental is the timing and magnitude of particular substorms that affect the *AL* index. There is an extensive literature on this subject already [e.g., *Rostoker et al.*, 1980; *Weimer*, 1994; *Kamide and Kokubun*, 1995; *Weimer*, 1995; *Rostoker*, 2002; *Sharma et al.*, 2003], and it is not the point of this paper to dwell on this but only to point out that this is probably the main cause of error in the 10-min *AL* index prediction.

[63] There is also error associated with the model parameters. The model parameters were found by minimizing the RMS error of the 10-min model results versus the 10-min averaged provisional *AL* index for 1995. Because the parameters are based on a limited amount of data and because of a certain randomness in the *AL* index, there is some error in the parameters compared to what one would expect given an infinite amount of data. We have not analyzed these errors in detail. Possibly the best way to analyze such errors would be to wait for more and better *AL* index data. Since late 1994, we have had almost continuous solar wind data. Unfortunately, the *AL* data are either provisional (1995) or, for later years, "quick look" [*Takahashi et al.*, 2004].

3.2. Out of Sample Comparison

[64] For the period 1997 through November 2001, the quick-look *AL* data have been available in digital form. We have used these data to test the model. Because the model is fit to the year 1995, we would expect it to behave slightly worse with respect to other years. In addition, the quick-look *AL* data are based on a limited number of stations. Instead of 12 stations, the quick-look *AL* for the years 1997 and 1998 is based on, at most, eight stations and often fewer, and the quick-look *AL* for the years 1999–2001 is based on, at most, nine stations but usually fewer. In

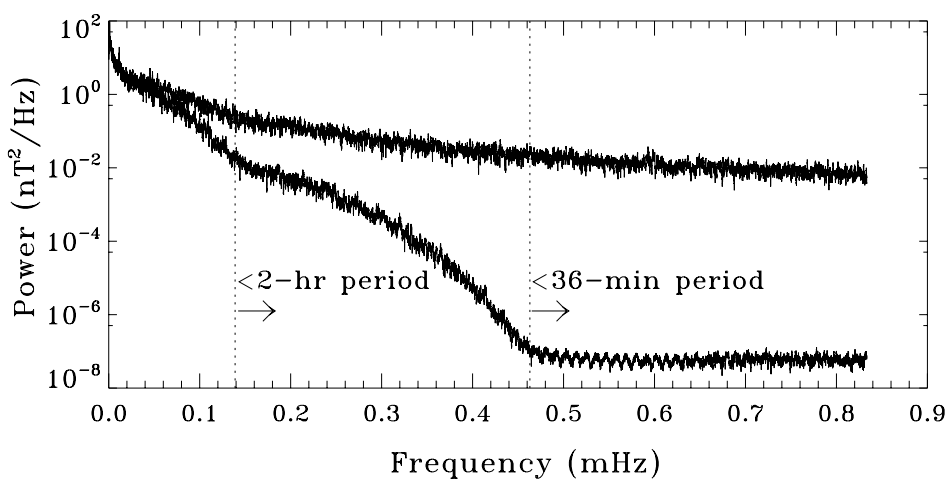

Figure 9. Thirteen-point averaged power of the Fast Fourier Transform from the modeled *AL* (lower curve) and the *AL* index (upper curve). The model has a much smaller response at higher frequencies corresponding to periods of shorter than two hours (0.14 mHz) and has practically no response for periods shorter than 36 min but has a response similar to the *AL* index for longer periods.

Table 1. A Summary of the Model Results Applied for 1997–2001[a]

Year	Correlation Coefficient	PE	Adjustment	Adjusted PE	RMS Error (AL_a), nT
1995	0.85	0.723	N/A	N/A	87.9
1997–2001	0.795	0.524	$AL_a = 0.735 * AL - 12.2$	0.631	88.0
1997	0.826	0.658	$AL_a = 0.909 * AL + 7.19$	0.682	70.0
1998	0.823	0.632	$AL_a = 0.812 * AL - 11.0$	0.677	86.8
1999	0.798	0.544	$AL_a = 0.769 * AL - 5.43$	0.637	89.3
2000	0.785	0.431	$AL_a = 0.683 * AL - 13.8$	0.616	93.5
2001	0.766	0.342	$AL_a = 0.621 * AL - 28.8$	0.587	91.9

[a]See text for detailed explanation.

addition, the data have substantial noise. There are spikes in the data as large as the order of 10,000 nT. We have visually inspected the quick-look data and interpolated the most obvious noisy data. This affected about 250 10-min intervals over the 5 years 1997–2001. Not all the noise was removed, and especially during disturbed periods, such noisy intervals can be difficult to detect. Nevertheless, we believe the remaining noise is not a significant factor; that is, it has substantially a <1% effect on the correlation coefficient or the prediction efficiency. The fewer number of reporting stations has a larger effect [*Takahashi et al.*, 2004]. Because *AL* is simply the magnitude of the variation of the H component of the magnetic field of the station with the largest negative magnitude, an *AL* index based on fewer stations will, at any one time, either be equal to what the 12-station *AL* would have been or be more positive; that is, it will have a smaller magnitude except for the rare cases when *AL* itself is actually positive.

[65] For the years 1997–2001, we found that our model gave a correlation coefficient of 0.795, a PE of 0.524, and an RMS error of 88.0 nT. We also examined the model's prediction for each year separately. This is summarized in Table 1. As expected, because the quick-look *AL* should have a smaller magnitude than the normal *AL*, the model overpredicts the magnitude of the quick-look *AL*. Thus we found we could get a better PE by making a simple linear adjustment to the predicted *AL*. This is shown in Table 1 as the "Adjustment." Such a linear adjustment does not affect the correlation coefficient but improves the PE and also gives an indication of how much less the quick-look magnitude may be because of its fewer stations. The overall RMS error for the years 1997–2001 is nearly the same as for 1995 (88.0 versus 87.9 nT) despite a lower correlation coefficient because auroral activity was at an above average level in 1995 because of recurrent high-speed, solar wind streams that occur during the declining phase of the solar cycle [*Li et al.*, 2001b] and because the RMS error scales approximately with auroral activity. Such adjustments, of course, should not be made when using the model as an indicator of real auroral activity.

[66] Looking at the individual years in Table 1 gives additional insight into the errors of our model. For the years 1997 and 1998, the correlation is good considering that we are using only quick-look *AL* data, but the correlation becomes progressively worse for later years. Examination of the data in more detail reveals that the additional error in the later years is due to very large errors during a few very large magnetic storms. While 1995 was active, it did not have the very large magnetic storms that occur near the maximum of the solar cycle. Typically, during the latter part of large magnetic storms, the model overpredicts the magnitude of *AL*. An example of such large errors is shown in Figure 10 for the 11 April 2001 magnetic storm ($Dst = -271$ nT). The overprediction of the quick-look *AL* could be due to the fact that the quick-look *AL* missed some of the auroral activity because of the limited number of stations (in Figure 10, the first 2 days are based on eight reporting stations, and the second 2 days are based on nine). However, the systematic behavior of this error suggests a more fundamental cause: It is likely that for large storms, the auroral oval expands equatorward of the reporting stations, though this requires further investigation. The systematic behavior of the error also suggests that the model can likely be improved for large magnetic storms, though at this time, we hesitate to do this on the basis of the quick-look data.

[67] For very large, long-lasting, solar wind drivers such as can occur during large magnetic storms, the model has some unfortunate features. As described in equation (14), the driver saturates, which can lead to a too small initial increase in the magnitude of the predicted *AL*. Later, because the solar wind driver is saturated, changes in the solar wind, as long as those changes still leave the driver saturated, are not reflected in the predicted *AL*. Under such conditions, the predicted *AL* oscillates around a large negative value because of the feedback provided by the time delayed terms in equation (11). This can lead to large errors since such oscillations may not necessarily be in phase with the oscillations in the measured *AL*.

3.3. Comparison With Previous Models

[68] Techniques for modeling and predicting geospace plasma phenomena including the *AL* index have recently been reviewed by *Vassiliadis* [2006]. The auroral indices and auroral activity have been intensively investigated. Nevertheless, it is difficult to find another model that can be applied to the same solar wind data set to compare directly with our model. Some models report predictions of the *AE* rather than the *AL* index, show comparisons for only short intervals, are more interested in the statistical properties of the auroral indices rather than in prediction, use different time resolution, or are just not explicit enough to be applied. A common problem has been the use of Ey (i.e., $Vx * bz$) as the sole solar wind driver.

[69] Some of the best predictions of the auroral indices have come from neural network models [*Gleisner and Lundstedt*, 1997, 2001; *Gavrishchaka and Ganguli*, 2001]. *Gleisner and Lundstedt* [1997] used solar wind density, velocity, and magnetic field as separate inputs into a neural network model to predict *AE* for the so-called "Bargatze"

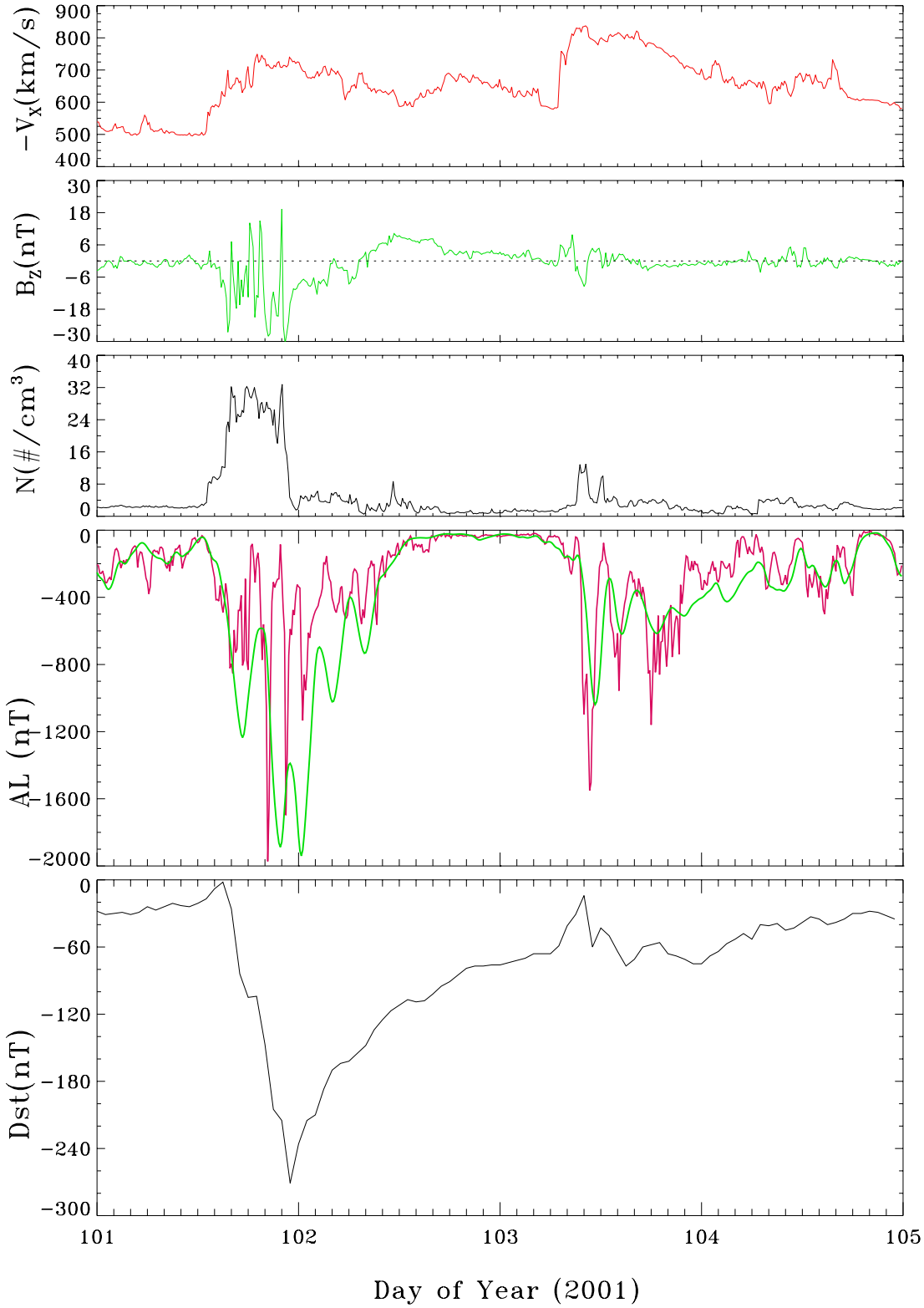

Figure 10. Relevant solar wind parameters and a comparison between the measured quick-look *AL* index (10-min averaged, red), the predicted *AL* index (green) from the complex model, and the measured *Dst* index for days 101–105 (11–15 April) of 2001.

data set [*Bargatze et al.*, 1985] which has been widely used in the modeling of *AE*. Their best correlation coefficient was almost 0.87. When using a single coupling function as an input to their model, they found that $n^{0.5} * V^3 *$ bz worked best and gave a correlation coefficient of about 0.84. We note that the large power dependence on the solar wind velocity relative to bz is similar to our result. *AE* is the difference between *AU* and *AL* (but essentially the sum of the magnitudes) and thus larger and so may be relatively easier to predict than *AL*. However, neural network models do not have an explicit formulation that is publicly available that can be used for direct comparison with other data. Gleisner and Lundstedt also reviewed previous results. They noted that the best results (correlation coefficient ~0.92 for *AE*) were reported by *Goertz et al.* [1993] but only for a limited and filtered set of data. *Vassiliadis et al.* [1995] used a nonlinear filter method to predict *AL* for the Bargatze data set with correlation coefficient of the order of 0.8, but this study did not provide a specific algorithm that can be applied for predictions.

[70] On short timescales, the *AL* index is not very predictable as we and others have shown. Partly because of this, much emphasis has been placed lately on the statistical properties of magnetosphere turbulence as reflected in the auroral indices and the possible implication of this turbulence on the nonlinear dynamics of magnetosphere [e.g., *Hnat et al.*, 2005] rather than on actual predictions of the auroral indices.

[71] Our method can be easily adapted for real-time predictions of auroral activity and can be used as a benchmark against which other methods can be measured.

3.4. Comparison of *AL* and *Dst*

[72] This work is partly a continuation of previous efforts to predict *Dst* index [*Temerin and Li*, 2002; 2006]. The solar wind driver for *Dst* and *AL* is the same, but the indices have substantially different appearances. The *AL* index can easily have a large response (~−1000 nT) to short timescale variations in the solar wind that barely affect the *Dst* index. Because of the fast decay of the *AL* index and the saturation of its driver term, long periods of intense southward IMF do not build up the *AL* index the way they do the *Dst* index (e.g., see Figure 1, around day 117). Because of this large and quick response of the *AL* index and because the timing of such large responses (i.e., substorms) is not exactly predictable, the *AL* index is also not as well predicted as the *Dst* index.

4. Summary and Conclusions

[73] We developed two empirical models to predict the 10-min resolution *AL* index using solar wind data for 1995. The prediction efficiency for a whole year for the complex model was 0.723, with a RMS error of 87.9 nT and a linear correlation coefficient of 0.850. A simpler model gave a prediction efficiency of 0.644, a RMS error of 99.6 nT, and a linear correlation coefficient of 0.803 and showed clearly the dependence of the *AL* index on solar wind parameters. The complex model predicts well the longer time-averaged behavior of the *AL* index but does not predict well the *AL* index on the scale of substorms, though the average effect of substorms is well predicted.

[74] Both models demonstrate which parameters in the solar wind are important in controlling the *AL* index. As is well known, the IMF and its direction mostly control magnetospheric activity, but the models indicate that solar wind velocity is more important than is usually assumed, while the solar wind density plays a negligible role for the *AL* index. The complex model also shows the relative importance of the equinoctial effect which enhances magnetospheric activity around the times of the equinoxes and the average diurnal and annual variations which are relatively small. In comparison with the *Dst* index, saturation effects and large decay rates prevent large events in the solar wind, such as long periods of intense southward IMF, from having a correspondingly large effect on the *AL* index. Timescales for decay of the *AL* index are less than an hour and decrease with the amplitude of *AL*. The *AL* index can easily have a large response (~−1000 nT) to short timescale variations in the solar wind that barely affect the *Dst* index. Our model can be used to understand better physical processes associated with auroral dynamics and for space-weather applications.

[75] **Acknowledgments.** This work was supported, in part, by NSF grants (ATM-0519207, -0549093and CISM: ATM-0120950) and NASA grant (NAG5-13518), and also in part by National Natural Science Foundation of China Grant 40125012 and the International Collaboration Research Team Program of the Chinese Academy of Sciences. KSO acknowledges financial support from Chungnam National University Research Foundation. We appreciate the effort by the science teams (WDC for Geomagnetism, Kyoto, Wind/3D, Wind/Mag) for providing the data and thank Steve Monk for helping with the computer programming and T. E. Sarris for making FFT for Figure 9. KSO thanks LASP for hosting his sabbatical from January 2004 to January 2005, when part of this work was done.

[76] Zuyin Pu thanks Alex Klimas and Gordon Rostoker for their assistance in evaluating this paper.

References

Ahn, B.-H., B. A. Emery, H. W. Kroehl, and Y. Kamide (1999), Climatological characteristics of the auroral ionosphere in terms of electric field and ionospheric conductance, *J. Geophys. Res.*, *104*, 10,031.

Ahn, B.-H., H. W. Kroehl, Y. Kamide, and E. A. Kihn (2000a), Universal time variations in the auroral electrojet indices, *J. Geophys. Res.*, *105*, 267.

Ahn, B.-H., H. W. Kroehl, Y. Kamide, and E. A. Kihn (2000b), Seasonal and solar cycle variations of the auroral electrojet indices, *J. Atmos. Sol.-Terr. Phys.*, *62*, 1301.

Allen, J. H., and H. K. Kroehl (1975), Spatial and temporal distributions of magnetic effects of auroral electrojets as derived from AE indices, *J. Geophys. Res.*, *80*, 3667.

Baker, D. N. (1986), Statistical analysis in the study of solar wind-magnetosphere coupling, in *Solar Wind-Magnetosphere Coupling*, edited by Y. Kamide and J. Slavin, p. 17, Springer, New York.

Baker, D. N., R. L. McPherron, T. E. Cayton, and R. W. Klebesadel (1990), Linear prediction filter analysis of relativistic electron properties at 6.6 R_E, *J. Geophys. Res.*, *95*, 15,133.

Baker, D. N., T. I. Pulkkinen, V. Angelopoulos, W. Baumjohann, and R. L. McPherron (1996), Neutral line model of substorms: Past results and present view, *J. Geophys. Res.*, *101*, 12,975.

Bargatze, L.F., D. N. Baker, R. L. McPherron, and E. W. Hones Jr. (1985), Magnetospheric impulse response for many levels of geomagnetic activity, *J. Geophys. Res.*, *90*, 6387.

Bargatze, L. F., R. L. McPherron, J. Minamora, and D. R. Weimer (2005), A new interpretation of the Weimer et al.'s solar wind propagation delay technique, *J. Geophys. Res.*, *110*, A07105, doi:10.1029/2004JA010902.

Baumjohann, W. and R. A. Treumann (1999), *Basic Space Plasma Physics*, p. 17, Imperial Coll. Press, London.

Burton, R. K., R. L. McPherron, and C. T. Russell (1975), An empirical relationship between interplanetary conditions and Dst, *J. Geophys. Res.*, *80*, 4204.

Chen, J., and A. S. Sharma (2006), Modeling and prediction of the magnetospheric dynamics during intense geospace storms, *J. Geophys. Res.*, *111*, A04209, doi:10.1029/2005JA011359.

Clauer, C. R. (1986), The technique of linear prediction filters applied to studies of solar wind-magnetosphere coupling, in *Solar Wind-Magnetosphere Coupling*, edited by Y. Kamide and J. Slavin, p. 39, Kluwer Acad., Norwell, Mass.

Clauer, C. R., and R. L. McPherron (1974), Mapping the local time-universal time development of magnetospheric substorms using mid-latitude magnetic observations, *J. Geophys. Res.*, *79*, 2811.

Cliver, E. W., Y. Kamide, and A. G. Ling (2000), Mountains versus valleys: Semiannual variation of geomagnetic activity, *J. Geophys. Res.*, *105*, 2413.

Davis, T. N., and M. Sugiura (1966), Auroral electrojet activity index AE and its universal time variations, *J. Geophys. Res.*, *71*, 785.

Gavrishchaka, V. V., and S. B. Ganguli (2001), Optimization of the neural-network geomagnetic model for forecasting large-amplitude substorm events, *J. Geophys. Res.*, *106*(A4), 6247, doi:10.1029/2000JA900137.

Gleisner, H., and H. Lundstedt (1997), Response of the auroral electrojects to the solar wind modeled with neural networks, *J. Geophys. Res.*, *102*, 14,269.

Gleisner, H., and H. Lundstedt (2001), Auroral electrojet predictions with dynamic neural networks, *J. Geophys. Res.*, *106*, 24,541.

Goertz, C. K., L.-H. Shan, and R. A. Smith (1993), Prediction of geomagnetic activity, *J. Geophys. Res.*, *98*, 7673.

Hernandez, J. V., T. Tajima, and W. Horton (1993), Neural net forecasting for geomagnetic activity, *Geophys. Res. Lett.*, *20*, 2707.

Hnat, B., S. C. Chapman, and G. Rowlands (2005), Scaling and a Fokker-Planck model for fluctuations in geomagnetic indices and comparison with solar wind epsilon as seen by Wind and ACE, *J. Geophys. Res.*, *110*(A8), A08206, doi:10.1029/2004JA010824.

Hones, E. W., Jr. (1979), Transient phenomena in the magnetotail and their relation to substorms, *Space Sci. Rev.*, *23*, 393.

Kamide, Y., and S. Kokubun (1995), Comments on the paper "Substorm time constants" by D. R. Weimer, *J. Geophys. Res.*, *100*, 5715.

Kamide, Y., and S. Kokubun (1996), Two-component auroral electrojet: Importance for substorm studies, *J. Geophys. Res.*, *101*, 13,027.

Kamide, Y., and G. Rostoker (2004), What is the physical meaning of the AE index?, *Eos Trans. AGU*, *85*(19), 188.

Klimas, A. J., D. N. Baker, D. A. Roberts, D. H. Fairfield, and J. Büchner (1992), A nonlinear dynamical analogue model of geomagnetic activity, *J. Geophys. Res.*, *97*, 12,253.

Klimas, A. J., D. N. Baker, D. Vassiliadis, and D. A. Roberts (1994), Substorm recurrence during steady and variable solar wind driving: Evidence for a normal mode in the unloading dynamics of the magnetosphere, *J. Geophys. Res.*, *99*, 14,855.

Klimas, A. J., D. Vassiliadis, and D. N. Baker (1998), Dst index prediction using data-derived analogues of the magnetospheric dynamics, *J. Geophys. Res.*, *103*, 20,435.

Li, X. (2004), Variations of 0.7–6.0 MeV electrons at geosynchronous orbit as a function of solar wind, *Space Weather*, *2*(3), S03006, doi:10.1029/2003SW000017.

Li, X., M. Temerin, D. N. Baker, G. D. Reeves, and D. Larson (2001a), Quantitative prediction of radiation belt electrons at geostationary orbit based on solar wind measurements, *Geophys. Res. Lett.*, *28*, 1887.

Li, X., D. N. Baker, S. G. Kanekal, M. Looper, and M. Temerin (2001b), SAMPEX Long Term Observations of MeV Electrons, *Geophys. Res. Lett.*, *28*, 3827.

Lyatsky, W., P. T. Newell, and A. Hamza (2001), Solar illumination as cause of the equinoctial preference for geomagnetic activity, *Geophys. Res. Lett.*, *28*, 2353.

McPherron, R. L., and G. Rostoker (1993), Comment on "Prediction of Geomagnetic Activity" by C. K. Goertz, Lin-Hua Shan, and R A. Smith, *J. Geophys. Res.*, *98*, 7685.

McPherron, R. L., C. T. Russell, and M. Aubry (1973), Satellite studies of magnetospheric substorms on August 15, 1968, 9. Phenomenological model for substorms, *J. Geophys. Res.*, *78*, 3131.

O'Brien, T. P., and R. L. McPherron (2000), An Empirical phase space analysis of ring current dynamics: Solar wind control of injection and decay, *J. Geophys. Res.*, *105*, 7707.

Rostoker, G. (2002), Why we have not yet solved the substorm problem, in *Proceedings of the Sixth International Conference on Substorms (ICS-6)*, edited by R. M. Winglee, p. 1, Univ. Wash., Seattle.

Rostoker, G., S.-I. Akasofu, J. Foster, R. A. Greenwald, Y. Kamide, K. Kawasaki, A. T. Y. Lui, R. L. McPherron, and C. T. Russell (1980), Magnetospheric substorms—Definition and signatures, *J. Geophys. Res.*, *85*, 1663.

Rostoker, G., T. D. Phan, and F. Pascal (1991), Inference of magnetospheric and ionospheric electrical properties from the decay of geomagnetic activity, *Can. J. Phys.*, *69*, 921.

Russell, C. T., and R. L. McPherron (1973), Semi-annual variation of geomagnetic, *J. Geophys. Res.*, *78*, 92.

Sharma, et al. (2003), The storm-substorm relationship: Current understanding and outlook, in *Disturbances in Geospace: The Storm–Substorm Relationship, Geophysical Monograph 142*, edited by A. S. Sharma, p. 1, AGU, Washington, D. C.

Shaw, R., (1984), *The Dripping Faucet as a Model Chaotic System*, The Sci. Frontier Express Ser., Aerial Press, Santa Cruz, Calif.

Shen, C., Z. Liu, and T. Kamei (2002), A physics-based study of the Dst–AL relationship, *J. Geophys. Res.*, *107*(A1), 1009, doi:10.1029/2001JA900121.

Takahashi, K., C. Meng, T. Kamei, T. Kikuchi, and M. Kunitake (2004), Near-real-time auroral electrojet index: An international collaboration makes rapid delivery of auroral electrojet index, feature, *Space Weather*, *2*(11), S11003, doi:10.1029/2004SW000116.

Temerin, M., and X. Li (2002), A new model for the prediction of Dst on the basis of the solar wind, *J. Geophys. Res.*, *107*(A12), 1472, doi:10.1029/2001JA007532.

Temerin, M., and X. Li (2006), Dst model for 1995–2002, *J. Geophys. Res.*, *111*, A04221, doi:10.1029/2005JA011257.

Vassiliadis, D. (2006), Systems theory for geospace plasma dynamics, *Rev. Geophys.*, *44*, RG2002, doi:10.1029/2004RG000161.

Vassiliadis, D., A. J. Klimas, D. N. Baker, and D. A. Roberts (1995), A description of the solar wind-magnetosphere coupling based on nonlinear filters, *J. Geophys. Res.*, *100*, 3495.

Weigel, R. S., A. J. Klimas, and D. Vassiliadis (2003), Solar wind coupling to and predictability of ground magnetic fields and their time derivatives, *J. Geophys. Res.*, *108*(A7), 1298, doi:10.1029/2002JA009627.

Weimer, D. R. (1994), Substorm time constants, *J. Geophys. Res.*, *99*, 11,005.

Weimer, D. R. (1995), Reply, *J. Geophys. Res.*, *100*, 5719.

Weimer, D. R., D. M. Ober, N. C. Maynard, M. R. Collier, D. J. McComas, N. F. Ness, C. W. Smith, and J. Watermann (2003), Predicting interplanetary magnetic field (IMF) propagation delay times using the minimum variance technique, *J. Geophys. Res.*, *108*(A1), 1026, doi:10.1029/2002JA009405.

X. Li, LASP/University of Colorado, 1234 Innovation Drive, Boulder, CO 80303-7814, USA. (lix@lasp.colorado.edu)

K. S. Oh, Department of Astronomy and Space Science, Chungnam National University, Daejeon, 305-764, Korea. (ksoh@cnu.ac.kr)

M. Temerin, 1062 Woodside Rd., Berkeley, CA 94708, USA.